RSC Advances

PAPER

Cite this: *RSC Adv.*, 2016, **6**, 84712

Water-soluble β-aminobisulfonate building blocks for pH and Cu^{2+} indicators†

Maria A. Cardona,[a] Marina Kveder,[b] Ulrich Baisch,[a] Michael R. Probert[c] and David C. Magri*[a]

Received 12th July 2016
Accepted 27th August 2016

DOI: 10.1039/c6ra17791c

www.rsc.org/advances

Two water-soluble phenyl β-aminobisulfonate ligands were synthesised and characterised by spectroscopic techniques including UV-visible absorption, electron paramagnetic resonance (EPR) and ^{1}H NMR spectroscopy. The acid–base and complexometric binding properties were studied in water and methanol, respectively. Single crystal X-ray crystallography was used to elucidate the solid-state properties. The pK_as of the phenyl β-aminobisulfonate **1** and methoxyphenyl β-aminobisulfonate **2** were evaluated to be 3.1 and 4.4, respectively. UV-visible, EPR and NMR spectroscopy provide direct evidence for complexation of **2** with Cu^{2+} in methanol due to coordination with the pendant methoxy moiety. The EPR and NMR data of **1** show evidence for some interaction, although no such conclusion could be derived from the UV-visible absorption spectra. The results highlight the potential of phenyl β-aminobisulfonates as building blocks for developing water-soluble pH and cation chemosensors.

Introduction

Molecular probes that are soluble in water are needed for practical biological and environmental applications.[1–5] Various strategies for imparting water solubility include supramolecular approaches such as inclusion complexes[6] and micellisation[7,8] in addition to molecular probes with charged fluorophores[9] or ionisable receptors.[10] Another common approach has been to append water-solubilising ligands such as aminoalkanesulfonate moieties.[11–17] The presence of sulfonate groups has been reported to improve the photophysical properties of dyes in solution by preventing aggregation and subsequently fluorescence quenching.[16] Furthermore, incorporation of alkanesulfonates widens the scope of dyes to biological[15] and green sustainability[18] applications without significantly affecting the absorption and emission properties.[13]

Aminoalkanesulfonates are used as ink-jet dyes,[19,20] surfactants and buffers.[20,21] Notable examples of buffers include 4-(2-hydroxyethyl)-1-piperazineethanesulfonic acid (HEPES), 3-(*N*-morpholino)propanesulfonic acid (MOPS), piperazine-*N*,*N*′-bis(2-ethanesulfonic acid) (PIPES) and morpholinoethane sulfonic acid (MES).[22–24] The use of sulfonated aniline derivatives as synthetic precursors provides a strategy for incorporating charged polar groups at the end of synthetic procedures,[13] and a way of tweaking the pK_a due to the electron-withdrawing nature of the sulfonate group.[24]

Contrary to conventional wisdom, aminoalkanesulfonates have been reported to complex with divalent metal ions, most notably, Ni^{2+}, Zn^{2+}, Co^{2+} and Cu^{2+}.[25] These metal ions have a tendency to form relatively stable metal complexes according to the Irving–Williams series. Cu^{2+} tends to form the most stable complexes of the first row transition metals.[26] In fact, Cu^{2+} has a notorious reputation for interfering with some of Good's buffers, particularly those with hydroxyl groups.[27] We hypothesised that incorporation of alkanesulfonate ligands might improve the water-solubility properties of small hydrophobic building blocks, as we observed with anthracene-based fluorescent chemosensors for H^+ and Fe^{3+},[28] as well as synergistically contributing to metal ion binding as observed with iminodiacetate[29] and β-aminobisphosphonate[30] moieties. Our curiosity was aroused by Gunnlaugsson's azobenzene chemosensor for Cu^{2+}, which uses iminodiacetate groups appended onto an *o*-methoxy aniline derivative.[31]

Herein we report the synthesis and characterisation of small aniline derivatives with alkanesulfonates ligands originally used as building blocks for azobenzene pH indicators.[32] Analytical methods including UV-visible absorbance, EPR and ^{1}H NMR spectroscopies were used to elucidate the binding properties of **1** and **2** as a function of pH and select biologically relevant metal ions, notably Cu^{2+}.

[a]*Department of Chemistry, Faculty of Science, University of Malta, Msida, MSD 2080, Malta. E-mail: david.magri@um.edu.mt; Fax: +356 2340 3320; Tel: +356 2340 2276*

[b]*Laboratory for Magnetic Resonances, Division of Physical Chemistry, Rudjer Boskovic Institute, Zagreb, Croatia*

[c]*School of Chemistry, Newcastle University, Newcastle upon Tyne, NE1 7RU, UK*

† Electronic supplementary information (ESI) available: ^{1}H NMR, ^{13}C NMR, IR spectra, HRMS and crystallographic data for compounds **1** and **2**. CCDC 1484207 and 1484351. For ESI and crystallographic data in CIF or other electronic format see DOI: 10.1039/c6ra17791c

Results and discussion

Compounds **1** and **2** were synthesised according to Scheme 1 by alkylation of aniline and *o*-anisidine, respectively, with two equivalents of sodium 2-bromoethane sulfonate in the presence of potassium iodide and potassium dihydrogen phosphate in DMF at 120 °C. On cooling, the products precipitated as white solids and were recrystallised from methanol in *ca.* 50% yields. The compounds were fully characterised by ^{1}H and ^{13}C NMR, infra-red (IR) and high resolution mass spectrometry (HRMS).

The ^{1}H NMR spectra in D_2O are shown in Fig. S1 and S2.† The ^{1}H NMR spectra of **1** exhibits five hydrogen atom resonances. The protons on the ethanesulfonate chains appear as two distorted triplets between 2.9 and 3.6 ppm. The protons nearest the nitrogen atom are more deshielded relative to the methylene protons nearest the sulfonate groups. The three *o*-methoxy protons of **2** appear as a sharp singlet at 3.85 ppm. The aromatic region is characterised by two higher order systems between 6.66–6.78 ppm corresponding to the *meta* protons and 7.16–7.24 ppm corresponding to the *ortho* and *para* protons in the case of **1** and between 7.00–7.12 ppm and 7.17–7.26 ppm in the case of **2**.

Further confirmation of the molecular structures of **1** and **2** were obtained by single crystal X-ray structure determination (Fig. 1 and 2). Crystals were prepared by slow diffusion of acetone into a concentrated aqueous solution of the compound. Compound **1** was crystallised as a potassium salt hydrate in the orthorhombic space group *Pnma* whereas **2** was crystallised as a hydrated potassium bromide double salt with the net formula $K_9[C_{11}H_{15}NO_7S_2]_4Br$ in the monoclinic space group $P2_1/c$. In both cases, the organic fraction of the crystal forms a precise column whereas the polar sulfonate substituents and potassium/bromide ions form a distinct second column. Fig. 1 and 2 show this very clearly. However, the arrangement of the aromatic fragments in the two crystal lattices is quite different.

In **1** the phenyl groups are neatly stacked in an orderly alternating paired zig-zag arrangement. The closest distance between the centroids of the aromatic rings is 5.346(1) Å. Thus no pi-stacking interactions are observed and no C(H)···centroid intermolecular interactions between the aromatic fragments

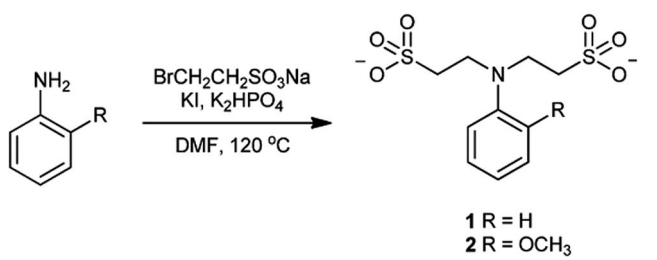

Scheme 1 Synthetic scheme for compounds **1** and **2**.

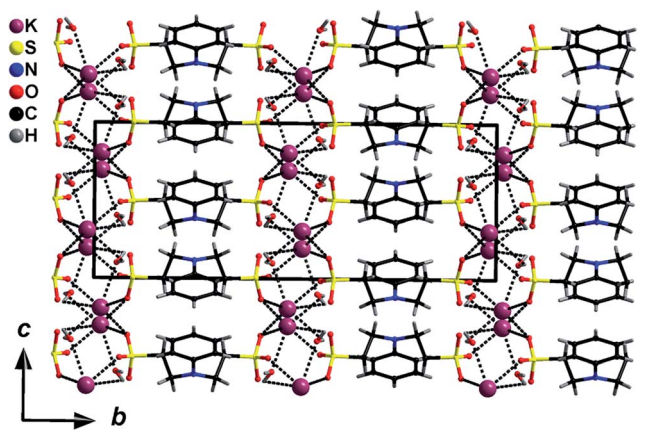

Fig. 1 Packing diagram of the crystal structure of **1** viewed along the cell axis *a*.

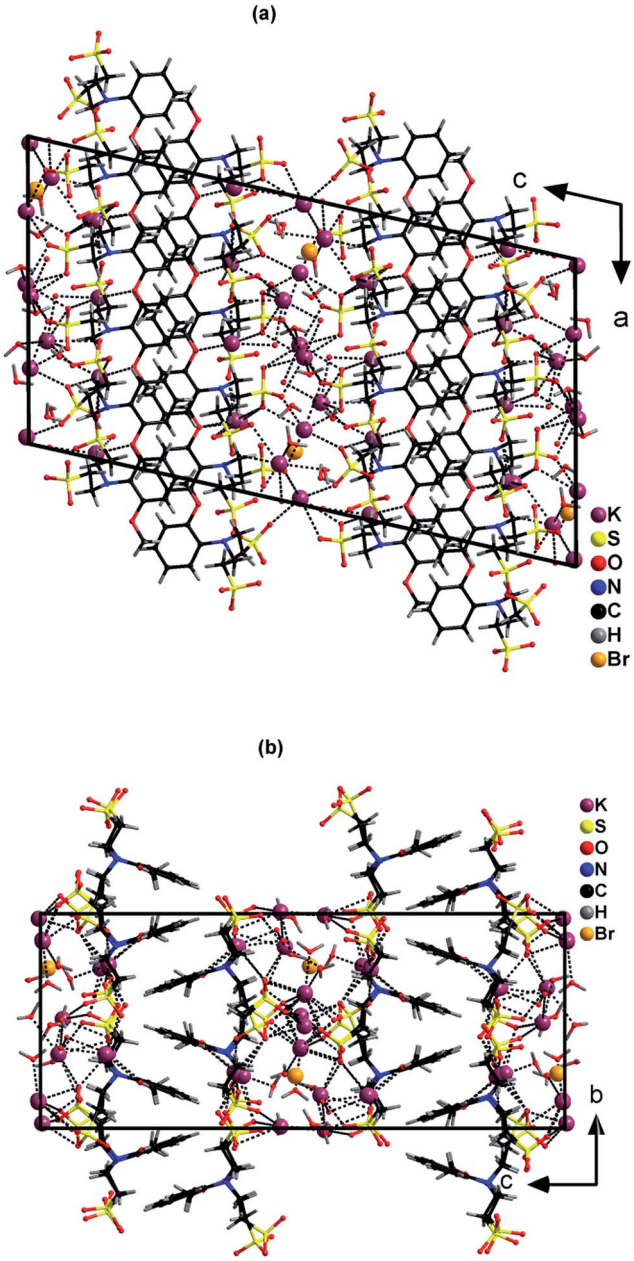

Fig. 2 Packing diagram of crystal structure of **2** viewed along (a) cell axis *b* and (b) cell axis *a*.

Table 1 UV-visible absorption spectroscopy and solubility parameters of 10^{-5} M **1** and **2** in water

Parameter	**1**	**2**
pK_a[a]	3.46	4.16
λ_{max} (nm)[b]	251, 296	246, 276
log ε (cm^{-1} M^{-1})[b]	4.03, 3.20	3.55, 3.41
λ_{max} (nm)[c]	251, 296	246, 276
log ε (cm^{-1} M^{-1})[c]	3.55, 3.41	2.79, 3.35
$p\beta_{Cu^{2+}}$[d]	—[e]	5.8[f]
log P[b]	-1.9 ± 0.6	-2.1 ± 0.6
log D[c]	-4.4 ± 0.6	-5.2 ± 0.6

[a] Estimated error for pK_a measurements is ± 0.10. Measurements done in duplicate. [b] At pH 8. [c] At pH 1.0. [d] Measured in methanol by UV-visible absorbance spectroscopy. [e] No significant change observed. [f] 2-Methoxy-*N*,*N*-diethylaniline has a value of 4.35.

were detected. The sulfonates form an intricate polymeric network on both sides of the phenyl groups with one counter ion and two water molecules per sulfonate group. The distances between two sulfur atoms and two nitrogen atoms on adjacent structures across the molecule are 6.89 Å and 4.75 Å, respectively.

In **2** the aromatic fragments are placed exactly upon each other in a zig-zag pattern one layer to the next (Fig. 2). Consequently, not only is the distance shorter between the centroids of the aromatic rings at 5.092(5) Å, but also there are surprisingly strong hydrogen bond interactions between the aromatic pi system and CH fragments of the neighbouring aromatic ring with a minimum C(H)···centroid distance of 2.48 Å. The distances between the two sulfur atoms, and two nitrogen atoms across the molecule on adjacent structures, are 6.94 Å and 6.86 Å, respectively. Hence, the N–N atom distance is greater with **2** compared to **1**.

The solubility properties of **1** and **2** were investigated prior to UV-visible absorption and NMR titration experiments by performing log P and log D calculations. The log P values were calculated to be -1.9 ± 0.6 and -2.1 ± 0.6 for **1** and **2**, respectively. In comparison, the log P values of diethylaniline and 2-methoxydiethylaniline are 3.4 ± 0.2 and 3.2 ± 0.3, respectively. The two charged sulfonate units are predicted to make **1** and **2** readily water solubility in agreement with the fact that at a pH greater than 5, both compounds are dianionic species. We were also interested in evaluating the solubility properties at lower pH once the anilinic nitrogen atom is protonated. Using the equation $\log D = \log P + \log[1/(1 + 10^{(pK_a - pH)})]$, and the experimentally determined pK_as of 3.46 and 4.16 (Table 1), the log D values at pH 3.0 were calculated to be -2.5 and -3.3 for **1** and **2**, respectively. These results predict that on protonation of the anilinic nitrogen atom, the molecules are more hydrophilic despite a decrease in the net negative charge. Protonation of the sulfonate groups is not expected. For example, the pK_a of ethanesulfonate is -1.68.[34]

Protonation studies by UV-visible absorption and ^{1}H NMR

The aromatic amines **1** and **2** exhibit bands in the UV-visible absorption region between 200 and 320 nm. More specifically, at alkaline pH compound **1** has peak maxima at 251 nm and 294 nm, and compound **2** at 243 nm and 276 nm. On addition of 0.1 M HCl, the maxima at 251 nm and 243 nm decrease for both compounds (Fig. 3). The longer wavelength band at *ca.* 295 nm decreased in the case of **1**, the 276 nm peak of **2** remained relatively consistent in intensity. The change in the absorbance of **1** and **2** as a function of pH is shown in Fig. 4. In both cases, a sigmoidal titration profile was observed over 2 log units. Application of the Henderson–Hasselbalch equation for absorbance spectroscopy, $pH = pK_a + \log[(A_{max} - A)]/[(A - A_{min})]$ allowed for the determination of the experimental pK_a values where the pK_a is the negative logarithm of the acid dissociation constant, and A_{max} and A_{min} are the maximum and minimum absorbances at a specific λ_{max} and A is the observed absorbance. From the intersection at the abscissa axes (Fig. 4: insets) pK_a values of 3.46 and 4.16 were determined for **1** and **2**, respectively.

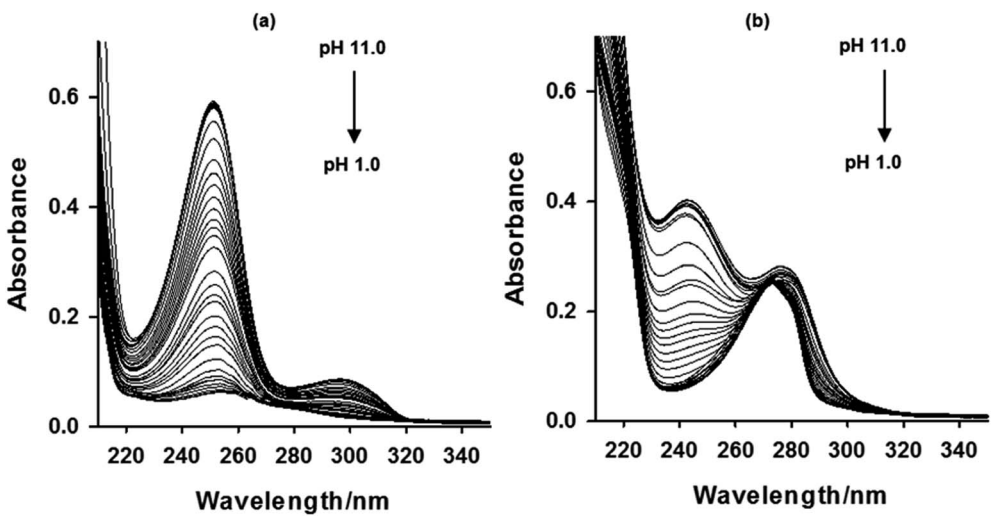

Fig. 3 UV-visible absorbance spectra of 60 μM **1** (a) and 100 μM **2** (b) in H_2O upon titration with 0.1 M HCl.

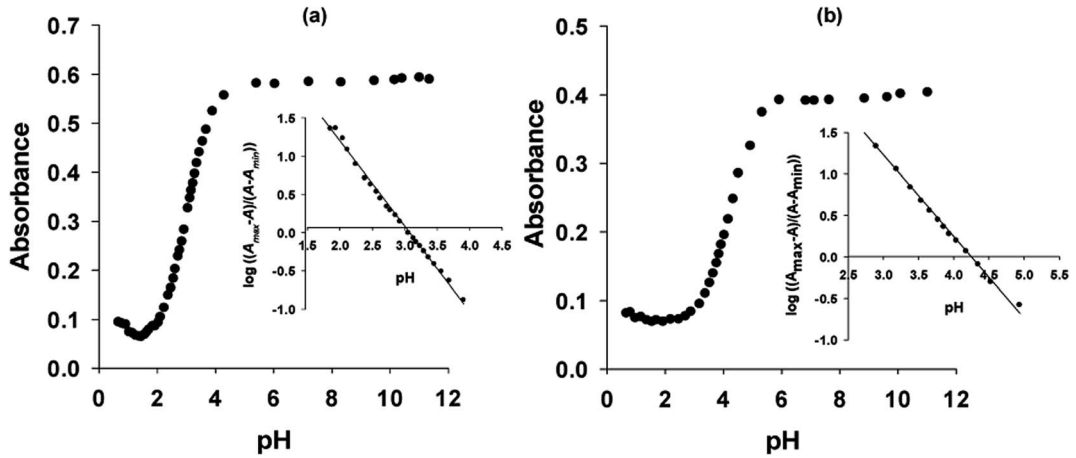

Fig. 4 Absorbance of 60 μM **1** at 251 nm (a) and 100 μM **2** at 246 nm (b) upon titration with 0.1 M HCl. Inset: determination of the pK_a by linearising the Henderson–Hasselbalch equation.

The protonation equilibria of **1** and **2** were also examined as a function of pD by ^{1}H NMR titration experiments (Fig. 5). At pD 8.75, **1** exhibits two broad triplets in the aliphatic region at 3.20 ppm and 3.80 ppm and two multiplets in the aromatic region at 6.80–7.00 ppm and 7.30–7.50 ppm, the latter assigned to two *ortho* protons and the former to the three other *meta* and *para* protons. As the concentration of acid increases, the chemical shift difference increases to $\Delta\sigma = 1.08$ ppm for the aliphatic resonances situated at 3.06 ppm and 4.14 ppm at pD 1.25. Additionally, the two multiplets in the aromatic region shift downfield and amalgamate between 7.60 ppm and 7.75 pm as the aromatic ring becomes electron-deficient on protonation. Similarly, **2** exhibits a near identical spectrum at neutral pD with the exception that an additional resonance is observed at 4.00 ppm due to the methoxy substituent. Titration of acid results in a similar perturbation of the aliphatic protons and a slight deshielding effect on the aromatic protons. The fact that the aliphatic protons nearest the nitrogen atom exhibit the largest chemical shifts confirms that protonation is indeed at the anilinic nitrogen atom rather than on the sulfonate or methoxy group.

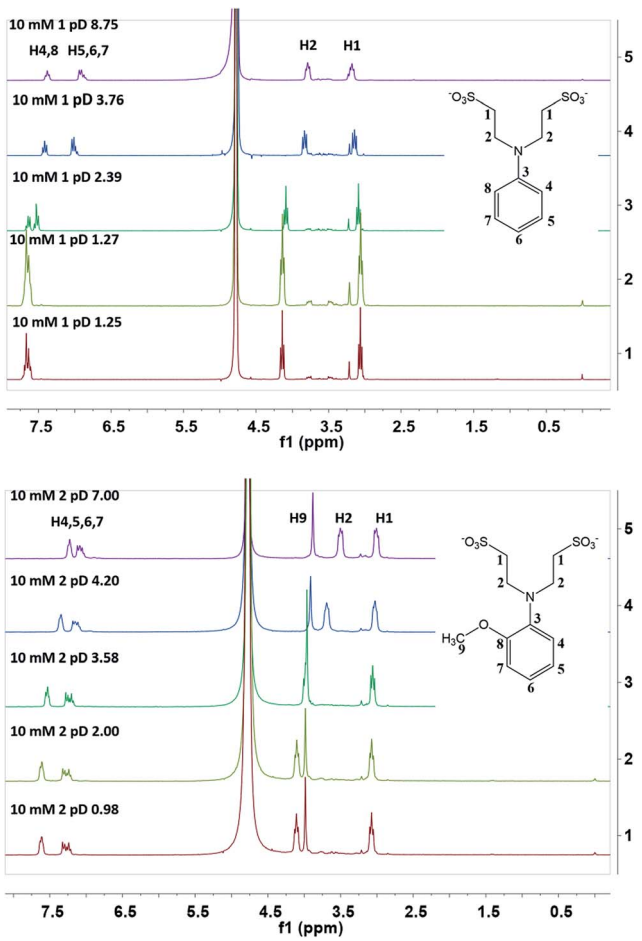

Fig. 5 ^{1}H NMR titration of **1** and **2** at 300 MHz in D_2O.

Metal ion studies by UV-visible absorption and ^{1}H NMR

UV-visible absorption spectroscopy was used to explore the ability of **1** and **2** complexing with the biologically relevant metal ions Na^+, K^+, Zn^{2+}, Fe^{3+} and Cu^{2+} in methanol. No change was observed in the spectrum of **1** upon addition of these metal ions. In the case of **2**, a new band was observed at 328 nm in the presence of Cu^{2+} (Fig. 6). Incremental addition of 1.5 mM Cu^{2+} to a 50 μM **2** in methanol induces a decrease in the peaks at 253 nm and 276 nm and a concomitant enhancement in the band at 329 nm. A plot of the absorbance *versus* the $-\log[Cu^{2+}]$ corresponds to a sigmoidal curve over two log units with a binding constant of 5.8 using a modified version of the Henderson–Hasselbalch equation (Fig. 7a). A Job's plot analysis with Cu^{2+} and **2** provides a 1 : 1 binding stoichiometry (Fig. 7b). Further insight into the role of the sulfonate groups was delineated by titrating 2-methoxy-*N*,*N*-diethylaniline with Cu^{2+} in methanol, which resulted in similar spectral changes and a log $\beta_{Cu^{2+}}$ of 4.35. It can be concluded that the sulfonates are not essential for coordination of Cu^{2+} in methanol. In water, however, no clear evidence for Cu^{2+} binding was observed by

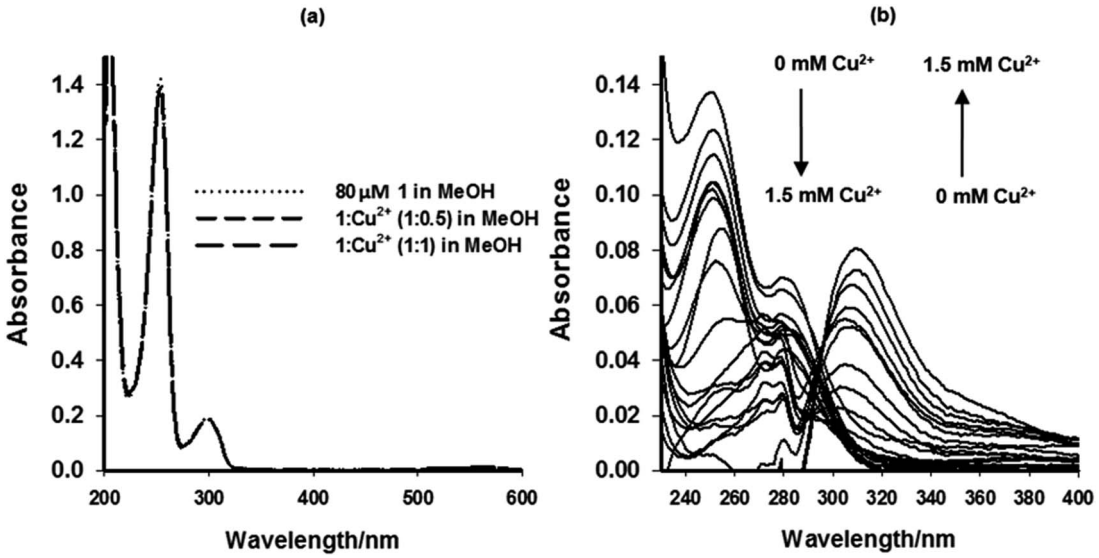

Fig. 6 UV-visible spectra of 80 μM **1** (a) and 50 μM **2** (b) in MeOH and upon addition of up to 1.5 mM Cu^{2+}.

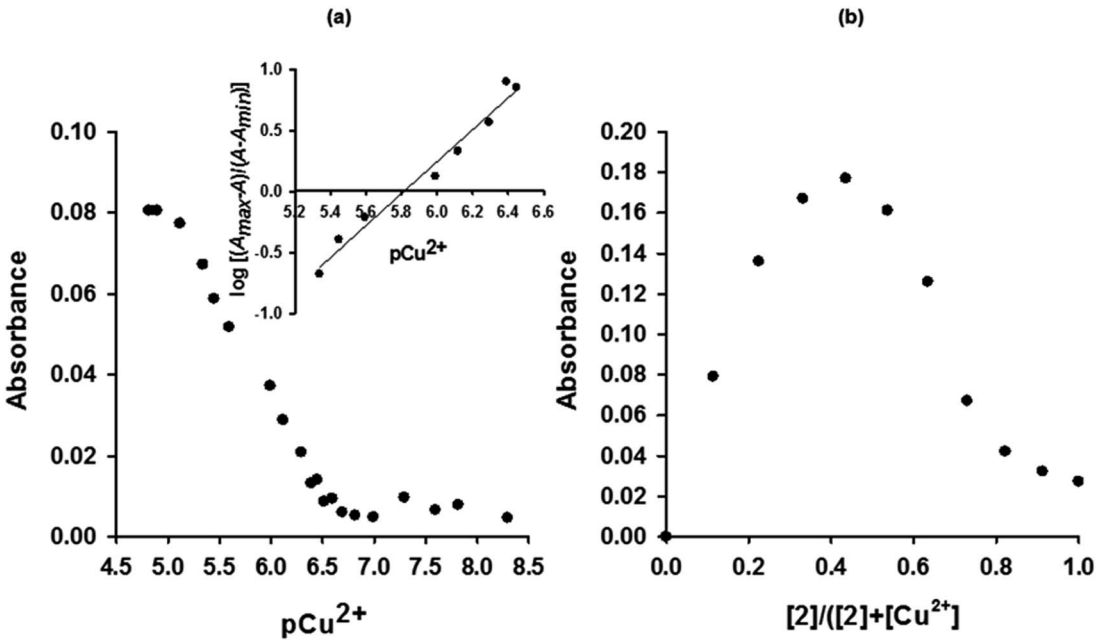

Fig. 7 (a) Absorbance at 309 nm upon titration of 50 μM **2** with Cu^{2+} in methanol. Inset: determination of pCu^{2+} of **2**; (b) Job's plot (separate experiment) obtained with a 10 mM solution of **2** at 328 nm.

UV-visible absorption spectroscopy with either **1** or **2** at these concentrations.

The ^1H NMR spectra of **1** and **2** are both affected by the presence of Cu^{2+} in CD_3OD (Fig. 8). On addition of 0.03 equivalent aliquots of copper(II) chloride (up to 0.09 equivalents) the aliphatic resonance of **1** broadens with loss of fine structure. The resonance originally at 3.8 ppm shifts slightly downfield and becomes submerged into the baseline. In the case of **2**, broadening and loss of fine structure is observed for all three aliphatic resonances including the methoxy signal. The aromatic hydrogen atom signals of **1** shift downfield by 0.1 ppm with loss of fine structure, although all three aromatic resonances are still evident. The aromatic signals of **2** are severely distorted in the presence of 0.09 equivalents of Cu^{2+}. These observations suggest that Cu^{2+} coordinates with both **1** and **2** to some extent in CD_3OD at millimolar concentrations. The resonances of the aliphatic protons nearest the nitrogen atom are distorted compared to the protons closest to the sulfonates. Therefore, the ligand–Cu^{2+} interaction must involve the anilinic nitrogen atom. Furthermore, the greater perturbation observed with **2** suggests the methoxy substituent strengthens the coordination interaction. We should reiterate, however, that the

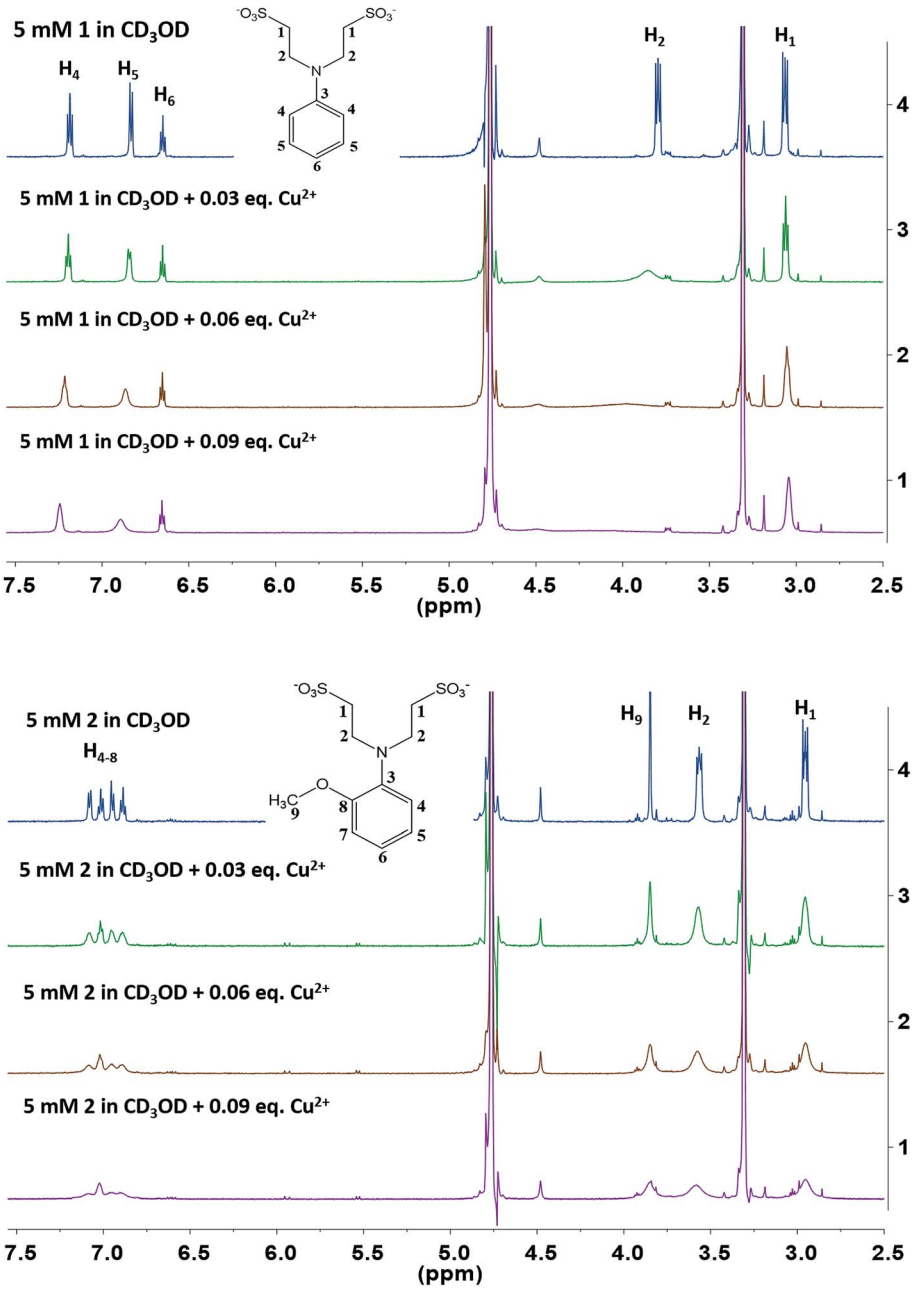

Fig. 8 ^{1}H NMR spectra of 5 mM **1** and **2** in CD_3OD upon titration with $CuCl_2$ at 600 MHz.

interaction between **1** and Cu^{2+} was not strong enough to induce observable changes in the UV-visible absorbance spectra.

EPR studies

As Cu^{2+} is paramagnetic, metal ion–ligand interactions with **1** and **2** were further investigated by EPR spectroscopy. The EPR spectrum of Cu^{2+} in methanol at room temperature exhibits a broad curve centred at $g \approx 2.2$ with the absence of any hyperfine lines (Fig. 9a). Upon addition of increasing aliquots of **2**, an increase in the EPR signal intensity was detected in addition to a slight decrease in the *g*-tensor value with concomitant change in the spectral line shape. This observation agrees with a Cu^{2+}–ligand interaction. Experiments attempted in water at room temperature showed a negligible change in the intensity of the broad spectral line centred at $g \approx 2.2$ confirming that any ligand–metal interaction in water is much weaker than in methanol.

Metal–ligand interactions between **1** and **2** with Cu^{2+} were also investigated in methanol at 80 K by rapidly cooling the sample.[35] At this temperature, methanol forms a glassy state resulting in a molecular state present at room temperature in a frozen state on the experimental time scale.[36] Contrary to methanol solution, water does not form a glassy state under these conditions due to the intrinsic nature of the specific water phase diagram,[37] and thus, cannot be studied in terms of the

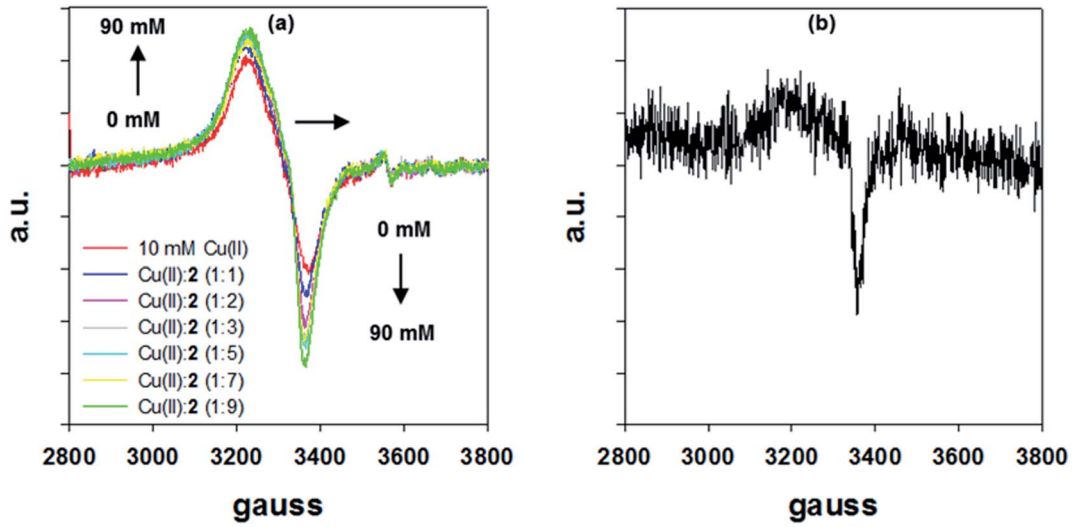

Fig. 9 (a) Room temperature EPR spectra of 10 mM Cu^{2+} in methanol upon addition of up to 90 mM (9 equivalents) **2**. (b) Subtracted EPR spectrum of 10 mM Cu^{2+} in methanol interacting with 10 mM **2** (subtraction of the original Cu^{2+} spectrum). 10 gauss = 1 mT.

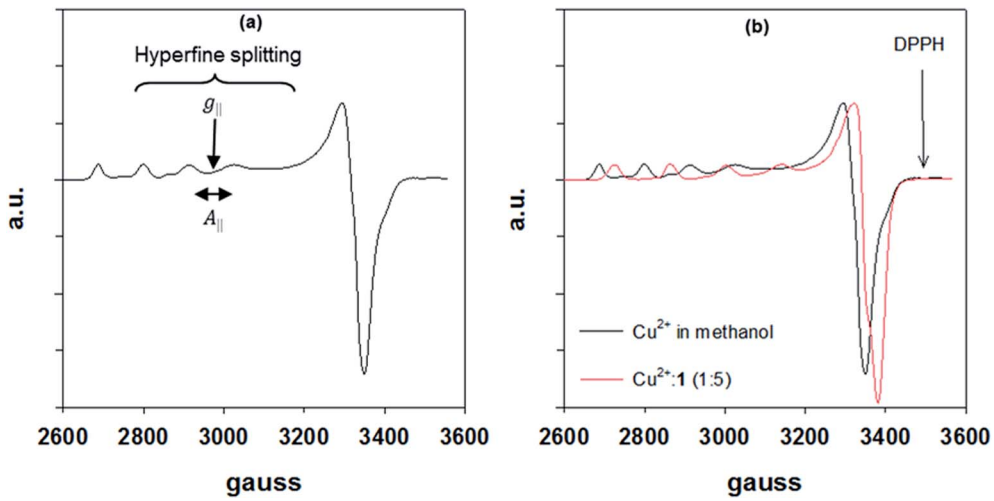

Fig. 10 (a) Spectrum of 10 mM Cu^{2+} in methanol at 80 K showing four hyperfine lines. $A_{\|}$ is taken from the difference between the second and third peak of the four hyperfine lines. $g_{\|}$ is obtained from the average magnetic field value at the middle of the second and third peak of the hyperfine splitting and converting this field value by comparison to DPPH (2,2-diphenyl-1-picrylhydrazyl); (b) spectrum of 10 mM Cu^{2+} in methanol overlaid over spectrum of 1 : 5 Cu^{2+} : **1**. 10 gauss = 1 mT.

cooled sample. The EPR spectrum of Cu^{2+} in a glassy state of methanol is shown in Fig. 10a. In the low field region below 3200 gauss, at least four hyperfine lines are resolved, which are ascribed to the hyperfine interaction of one unpaired electron ($S = 1/2$) with the Cu^{2+} nucleus ($I = 3/2$). The order of the g-tensor values are $g_{\|} > g_{\perp} > g_{\text{free electron}}$ ($g_{\text{free electron}} = 2.0023$), which is suggestive of a tetragonally distorted octahedron environment of Cu^{2+}.[38] The spectral parameters $A_{\|}$ and $g_{\|}$ for Cu^{2+} in methanol are 11.4 and 2.44, respectively at 80 K (Table 2).[39] Solutions of Cu^{2+} plus ligand resulted in significant differences in both the $A_{\|}$ and $g_{\|}$ values: 14.0 and 2.37, and 14.1 and 2.37, respectively, with **1** and **2**. These results were obtained by spectral simulation of the EPR data for Cu^{2+}, and Cu^{2+} with each ligand using EasySpin software package[40] (Fig. 10b). Specifically, in the presence of ligand an increase in the hyperfine splitting ($\Delta A_{\|} \approx +2.5$ mT) and a decrease in the g-value ($\Delta g_{\|} \approx -0.07$) can be noticed as compared to the Cu^{2+} spectrum in the absence of ligands. These observations could

Table 2 Values for $A_{\|}$ (mT) and $g_{\|}$ for the spectrum of 10 mM Cu^{2+} in methanol and in the presence of 50 mM **1** and **2** at 80 K

Spectrum[a]	$A_{\|}$, mT	$g_{\|}$
Cu^{2+}	11.4	2.44
Cu^{2+} + **1**	14.0	2.37
Cu^{2+} + **2**	14.1	2.37

[a] In methanol with 10 mM Cu^{2+} and 50 mM **1**or **2**.

be either a consequence of endogenous ligand displacement by a more negative ligand, such as the displacement of methanol and/or water by sulfonate, or due to elongation of the octahedral symmetry of Cu^{2+} due to an adjustment of the hydration shell surrounding Cu^{2+}.[41]

Conclusions

We have synthesised two water-soluble ligands with ethanesulfonate units. Metal ion coordination with both **1** and **2** is weak in water, but is dramatically improved in methanol, most notably with **2**. Proof for strong binding between Cu^{2+} and **2** comes from the UV-visible absorption spectra and the Job's plot analysis due to the additional *o*-methoxy group.[42] EPR measurements confirm that the environment about Cu^{2+} is perturbed by the presence of both **1** and **2** in methanol at 80 K. However, noticeable EPR spectral changes are observed between **2** and Cu^{2+} even at room temperature. The EPR, NMR and UV-visible absorption spectroscopic data provide convincing evidence for a strong interaction between **2** and Cu^{2+} in methanol. We anticipate that these results should provide further insight into the design of building blocks for new metal ion receptors with synergistic binding and water solubility properties.

Experimental

Chemicals

Aniline and 2-methoxyaniline were purchased from Hopkins & Williams. Aniline was distilled under reduced pressure over KOH pellets. Sodium bromoethanesulfonate was purchased from Sigma-Aldrich. *N*,*N*-Dimethylformamide, 1,4-dioxane were purchased from Lab Scan. Dipotassium hydrogen phosphate, hydrochloric acid, potassium iodide and sodium sulfite were purchased from Carlo Erba. All other chemicals were used as received unless stated otherwise.

Instrumentation

^{1}H and ^{13}C NMR spectra were recorded at room temperature on a Bruker AM 250 NMR spectrometer equipped with a ^{1}H/^{13}C 5 mm dual probe at 250.1 and 62.9 MHz, respectively, with DMSO-d_6 or D_2O as solvents. ^{1}H NMR titrations with Cu^{2+} concentration were performed at room temperature on a Bruker Avance 600 MHz spectrometer equipped with a 1H BBO BB 5 mm probe operating at 600.1 MHz. ^{1}H NMR titrations with pH were performed at room temperature on a DD2 Agilent Technology NMR spectrometer at a frequency of 297.8 MHz. Chemical shifts are reported in ppm *versus* tetramethylsilane or the residual solvent peak (δH = 4.79 ppm in the case of the HDO residual peak in D_2O). ^{13}C NMR spectra were recorded in D_2O containing 1 μl of 1,4-dioxane and referenced *versus* the CH_2 peak at δ 67.19 ppm.

EPR spectra carried out at 293 K were recorded in glass capillaries (inner diameter of 1 mm) on an X-band Varian E-109 spectrometer equipped with a Bruker variable temperature control unit. Low temperature measurements were performed in quartz tubes (inner diameter of 4 mm) with a Bruker E-580 Fourier transform continuous wave (FT/CW) X-band spectrometer equipped with an Oxford Instruments temperature unit at 80 K with liquid nitrogen as the cryogen. Magnetic parameters were measured by field calibration with diphenylpicrylhydrazyl (DPPH, g = 2.0036). The simulation of experimental low-temperature data were performed with EasySpin software package.

Infrared (IR) spectra were recorded as KBr discs on a Shimadzu IR Affinity-1 spectrophotometer calibrated using the 1601 cm^{-1} polystyrene absorption peak and reported in wavenumbers (cm^{-1}). Melting points were recorded on a Griffin melting point apparatus and are uncorrected. UV-visible absorption spectra were recorded on a Jasco V-650 spectrophotometer and spectra reported in nm. pH measurements were carried out using a Hanna instrument pH 210 microprocessor pH meter calibrated with standard buffer solutions at pH 4.00 and 7.00. HRMS spectra were conducted by Medac LTD. Log P values were calculated using Chemsketch© product version 12.01. Thin-layer chromatography silica TLC plates on Al foil with 60 Å pore diameter size silica gel were visualised with a handheld lamp using 254 and 365 nm light.

X-ray crystallographic data for **1** and **2** were collected on an Oxford Diffraction Gemini A Ultra diffractometer at 150 K using Cu K_α radiation (λ = 1.54184 Å) and an Atlas detector. Analytical absorption correction using analytical numeric absorption corrections using a multifaceted crystal model based on expressions derived by R.C. Clark & J.S. Reid[43] were applied based on symmetry-equivalent and repeated reflections. Structures were solved by direct methods and refined on all unique F^2 values, with anisotropic non-H atoms and constrained riding isotropic H atoms. Compound **2** showed intrinsic multiple non-merohedric twinning resulting in refinement factors of lower quality with wR_2 factors >30% and R_{int} of *ca.* 16%. Best results were obtained when one individuum was extracted and twin corrected. Data reduction and absorption correction was carried out using the CrysAlisPro[44] software. Programs were CrysAlisPro[44] for data collection, integration, and absorption corrections as well as OLEX2 [45] or SHELXTL and SHELXL[46] for structure determination and refinement. Full details about crystallographic experimental information is provided as ESI, together with a list of bond distances and angles.†

Synthesis

Compounds **1** and **2** were synthesised using a modified literature procedure.[31] 2-Methoxy-*N*,*N*-diethylaniline was synthesised from alkylation of *o*-anisidine with bromoethane as described in literature[33] and purified by column chromatography (95 : 5 hexane : ethyl acetate).

2-[Phenyl(2-sulfonatoethyl)amino]ethane-1-sulfonate (1). Sodium 2-bromoethanesulfonate (4.58 g, 21.7 mmol) and potassium iodide (2.09 g, 13.0 mmol) were dissolved in 150 ml of warm DMF in a two-necked 250 ml round-bottomed flask in an oil bath and fitted with a reflux condenser. Distilled aniline (1.0 ml, 11 mmol) and dipotassium hydrogen phosphate (4.27 g, 25.0 mmol) were added to the reaction mixture. The suspension

was heated at 120 °C for 72 hours. On cooling a white precipitate was collected by vacuum filtration. Recrystallisation from 8 : 2 methanol/water afforded a white solid in 50% yield. On prolonged exposure to the atmosphere, the solid turns a pale pink-violet colour. $R_f = 0.56$ (1 : 1 $CHCl_3$: MeOH); m.p. 300–303 °C; ^{1}H NMR (250 MHz, D_2O, ppm): δ 2.96–3.50 (m, 4H, NCH_2CH_2), 3.58–3.66 (m, 4H, NCH_2CH_2), 6.66–6.78 (m, 3H, Ar*H*), 7.16–7.24 (m, 2H, Ar*H*); ^{13}C NMR (63 MHz, D_2O, ppm): δ 47.0, 48.3, 114.1, 118.6, 130.5, 147.1; IR (KBr disc, cm^{-1}): 3456, 3419, 3065, 3048, 2941, 2903, 1670, 1601, 1501, 1416, 1369, 1285, 1221, 1198, 1169, 1042, 1005, 953, 810; UV-vis (H_2O, pH 11.0, nm): λ_{max} 251 ($\varepsilon = 10\,800$ cm^{-1} mol^{-1} L), 296 ($\varepsilon = 1580$ cm^{-1} mol^{-1} L); UV-vis (λ_{max}, H_2O, pH 1.5, nm): λ_{max} 251 ($\varepsilon = 1160$ cm^{-1} mol^{-1} L), 296 ($\varepsilon = 350$ cm^{-1} mol^{-1} L); MS (ES-TOF) *m*/*z* (%): 309 ([M + 2H], 15), 308 ([M + H], 100), 200 (7); HRMS calcd for $C_{10}H_{14}NO_6S_2$ 308.0263 [M + H], found 308.0273.

2-[(2-Methoxyphenyl)(2-sulfonatoethyl)amino]ethane-1-sulfonate (2). A similar protocol was used for the synthesis of **2** using 3.18 g (15.1 mmol) of sodium 2-bromoethane sulfonate, 2.44 g (14.7 mmol) of potassium iodide, 0.80 ml (7.1 mmol) of *o*-anisidine and 2.59 g (14.8 mmol) of anhydrous dipotassium hydrogen phosphate. The reaction was heated at 120 °C for 120 hours resulting in a blue-coloured suspension. On cooling to room temperature, a blue solid was collected in a grade 4 sintered glass crucible and washed with acetone. Recrystallisation from methanol yielded **2** in 40% yield. $R_f = 0.56$ (1 : 1 $CHCl_3$: MeOH); m.p. 268–270 °C; ^{1}H NMR (250 MHz, D_2O, ppm): δ 2.94–3.04 (m, 4H, NCH_2CH_2), 3.43–3.53 (m, 4H, NCH_2CH_2), 3.85 (s, 3H, OCH_3), 7.00–7.12 (m, 2H, Ar*H*), 7.17–7.26 (m, 2H, Ar*H*); ^{13}C NMR (63 MHz, D_2O, ppm): δ 48.6, 48.9, 56.0, 113.1, 121.7, 123.1, 126.2, 136.6, 154.6.; IR (KBr disc, cm^{-1}): 3462 (br), 3067, 2940, 2841, 1653, 1501, 1196 (br), 1043, 750; UV-vis (H_2O, pH 11.0, nm): λ_{max} 246 ($\varepsilon = 3580$ cm^{-1} mol^{-1} L), 276 ($\varepsilon = 2520$ cm^{-1} mol^{-1} L), 600 ($\varepsilon = 452$ cm^{-1} mol^{-1} L); UV-vis (H_2O, pH 1.6, nm): λ_{max} 246 ($\varepsilon = 612$ cm^{-1} mol^{-1} L), 276 ($\varepsilon = 2230$ cm^{-1} mol^{-1} L), 600 ($\varepsilon = 452$ cm^{-1} mol^{-1} L); MS (ES-TOF) *m*/*z* (%): 362 ([M + Na + H], 24), 361 ([M + Na], 30), 339 ([M + 2H], 18), 338 ([M + H], 100), 315 (20); HRMS calcd for $C_{11}H_{16}NO_7S_2$ 338.0369 [M + H], found 338.0368.

Acknowledgements

We acknowledge financial support from the University of Malta, the Strategic Educational Pathways Scholarship (Malta) part-financed by the European Social Fund (ESF) under Operational Programme II, and European Cooperation in Science and Technology (COST Action CM1005 "Supramolecular Chemistry in Water"). We extend our gratitude to Prof. Robert M. Borg at the University of Malta, and Dr. Damjan Makuc and Prof. Janez Plavec at the Slovenian NMR Centre in Ljubljana for assistance with ^{1}H NMR experiments. The authors thank the Diamond Light Source for access to beamline I19.

References

1 X. Li, X. Gao, W. Shi and H. Ma, *Chem. Rev.*, 2014, **114**, 590.
2 M. Formica, V. Fusi, L. Giorgi and M. Micheloni, *Coord. Chem. Rev.*, 2012, **256**, 170.
3 A. Bianchi, E. Delgado-Pinar, E. García-Espaňa, A. Giorgi and F. Pina, *Coord. Chem. Rev.*, 2014, **260**, 156.
4 D. Sareen, P. Kaur and K. Singh, *Coord. Chem. Rev.*, 2014, **265**, 125.
5 K. P. Carter, A. M. Young and A. W. Palmer, *Chem. Rev.*, 2014, **114**, 4564.
6 R. N. D'souza, U. Pischel and W. M. Nau, *Chem. Rev.*, 2011, **111**, 7941.
7 P. Pallavicini, Y. A. Diaz-Fernandez and L. Pasotti, *Coord. Chem. Rev.*, 2009, **253**, 2226.
8 *Supramolecular Systems in Biomedical Fields*, ed. H.-J. Schneider, RSC Publishing, London, UK, 2013.
9 (*a*) S. Basili, T. Del Giacco, F. Elisei and R. Germani, *Org. Biomol. Chem.*, 2014, **12**, 6677; (*b*) J. T. Hutt, J. Jo, A. Olasz, C.-H. Chen, D. Lee and Z. D. Aron, *Org. Lett.*, 2012, **14**, 3162; (*c*) W. F. Jager, T. S. Hammink and O. van den Berg, *J. Org. Chem.*, 2010, **75**, 2169; (*d*) O. van den Berg, W. F. Jager and S. J. Picken, *J. Org. Chem.*, 2006, **71**, 2666; (*e*) L. Li, J. Han, B. Nguyen and K. Burgess, *J. Org. Chem.*, 2008, **73**, 1963.
10 (*a*) A. P. de Silva, H. Q. N. Gunaratne and G. E. M. Maguire, *J. Chem. Soc., Chem. Commun.*, 1994, 1213; (*b*) T. Gunnlaugsson and J. P. Leonard, *J. Chem. Soc., Perkin Trans. 2*, 2002, 1980; (*c*) T. Gunnlaugsson, M. Nieuwenhuyzen, L. Richard and V. Thoss, *J. Chem. Soc., Perkin Trans. 2*, 2002, 141.
11 (*a*) J. Jose and K. Burgess, *J. Org. Chem.*, 2006, **71**, 7835; (*b*) J. Han and K. Burgess, *Chem. Rev.*, 2010, **110**, 2709.
12 C. Bouteiller, G. Clave, A. Bernardin, B. Chipon, M. Massonneau, P. Renard and A. Romieu, *Bioconjugate Chem.*, 2007, **18**, 1303.
13 B. Chipon, G. Clave, C. Bouteiller, M. Massonneau, P.-Y. Renard and A. Romieu, *Tetrahedron Lett.*, 2006, **47**, 8279.
14 R. M. El-Shishtawy, A. S. Oliviera, P. Almeida, D. P. Ferreira, D. S. Conceiçao and L. F. Vieira Ferreira, *Molecules*, 2013, **18**, 5648.
15 R. M. El-Shishtawy and P. Almeida, *Tetrahedron*, 2006, **62**, 7793.
16 N. Ho, R. Weissleder and C. Tung, *Tetrahedron*, 2006, **62**, 578.
17 Z. Zhang and S. Achilefu, *Chem. Commun.*, 2005, 5887.
18 H. Liang, S. K. Das, J. R. Galvan, S. M. Sato, Y. Zhang, L. N. Zakharov and A. L. Rheigold, *Green Chem.*, 2005, **7**, 410.
19 K. Yamakawa, A. Suzuki, K. Takahisa, T. Mikoshiba and H. Naruse, *Jpn. Kokai Tokkyo Koho*, 2002, JP 20022338837 A 2001127.
20 G. Hellong, J. Hagemann and B. Weber, *Eur. Pat. Appl.*, 1998, EP 882600 A2 19981209.
21 F. Tomiyoshi, K. Sadakatsu and S. Kiyotaka, *Jpn. Kokai Tokkyo Koho*, 1992, JP 04360862 A 19921214.
22 N. E. Good, G. D. Winget, W. Winter, T. N. Connolly, S. Izawa and R. M. M. Singh, *Biochemistry*, 1966, **5**, 467.

23 R. D. Long, N. P. Hilliard Jr, S. A. Chhatre, T. V. Timofeeva, A. A. Yakovenko, D. K. Dei and E. A. Mensah, *Beilstein J. Org. Chem.*, 2010, **6**, 31, DOI: 10.3762/bjoc.6.31.

24 M. Nunes de Jesus, N. Hioka, W. Ferreira da Costa and F. Maionchi, *J. Phys. Org. Chem.*, 2002, **15**, 617.

25 (*a*) S. Garcia-Gallego, J. S. Rodriguez, J. L. Jimenez, M. Cangiotti, M. F. Ottaviani, F. Ma., M. A. M. Fernandez, R. Gomez and F. J. de la Mata, *Dalton Trans.*, 2012, **41**, 6488; (*b*) S. Garcia-Gallego, M. J. Serramia, E. Arnaiz, L. Diaz, M. A. Munoz-Fernandez, P. Gomez-Sal, M. F. Ottaviani, R. Gomez and F. J. de la Mata, *Eur. J. Inorg. Chem.*, 2011, 1657.

26 H. Irving and R. J. P. Williams, *J. Chem. Soc.*, 1953, 3192.

27 Q. Yu, A. Kandegedara, Y. Xu and D. B. Rorabacher, *Anal. Biochem.*, 1997, **253**, 50.

28 M. A. Cardona, C. J. Mallia, U. Baisch and D. C. Magri, *RSC Adv.*, 2016, **6**, 3783.

29 (*a*) T. Gunnlaugsson, T. C. Lee and R. Parkesh, *Org. Lett.*, 2003, **5**, 4065; (*b*) R. Parkesh, T. C. Lee and T. Gunnlaugsson, *Org. Biomol. Chem.*, 2007, **5**, 310; (*c*) T. Gunnlaugsson, T. C. Lee and R. A. Parkesh, *Org. Biomol. Chem.*, 2003, **1**, 3265.

30 (*a*) J. F. Callan, S. Kamila, N. Singh, R. C. Mulrooney, M. MacKay, M. C. Cronin, J. Dunn and D. G. Durham, *Supramol. Chem.*, 2009, **21**, 643; (*b*) S. Kamila, J. F. Callan, R. C. Mulrooney and M. Middleton, *Tetrahedron Lett.*, 2007, 7756.

31 T. Gunnlaugsson, J. P. Leonard and N. S. Murray, *Org. Lett.*, 2004, **6**, 1557.

32 M. A. Cardona and D. C. Magri, *Tetrahedron Lett.*, 2014, **55**, 4559.

33 R. L. Bent, J. C. Dessloch, F. C. Duennebier, D. W. Fassett, D. B. Glass, T. H. James, D. B. Julian, W. R. Ruby, J. M. Snell, J. H. Sternerm, J. R. Thirtle, P. W. Vittum and A. Weissberger, *J. Am. Chem. Soc.*, 1951, **73**, 3100.

34 J. P. Guthrie, *Can. J. Chem.*, 1978, **56**, 2342.

35 M. J. Brugmans and W. L. Vos, *J. Chem. Phys.*, 1995, **103**, 2661.

36 M. D. Ediger, C. A. Angell and S. R. Nagel, *J. Phys. Chem.*, 1996, **100**, 13200.

37 (*a*) C. A. Angell, *Science*, 2008, **319**, 582; (*b*) M. Valko, P. Pelikán, S. Biskupič and M. Mazúr, *Chem. Pap.*, 1990, **44**, 805.

38 S. Deshpande, D. Srinivas and P. Ratnasamy, *J. Catal.*, 1999, **188**, 261.

39 F. Khattou, G. Aptel, J.-V. Zanchetta, D. J. Jones, B. Deroide and J. Rozière, *J. Mater. Chem.*, 1999, **9**, 2453.

40 S. Stoll and A. Schweiger, *J. Magn. Reson.*, 2006, **178**, 42.

41 (*a*) V. Bassetti, L. Burlamacchi and G. Martini, *J. Am. Chem. Soc.*, 1979, **101**, 5471; (*b*) D. Rousseau, *Structural and Resonance Techniques in Biological Research*, Academic Press, UK, 1984.

42 R. A. Schultz, B. D. White, K. A. Dishong, W. Arnold and G. W. Gokel, *J. Am. Chem. Soc.*, 1985, **107**, 6659.

43 R. C. Clark and J. S. Reid, *Acta Crystallogr., Sect. A: Found. Crystallogr.*, 1995, **51**, 887.

44 CrysAlisPro, Version 1.171.38.41, ed., Rigaku OD, 2015, p. Xcalibur CCD system.

45 O. V. Dolomanov, L. J. Bourhis, R. J. Gildea, J. A. K. Howard and H. Puschmann, *J. Appl. Crystallogr.*, 2009, **42**, 339.

46 (*a*) G. M. Sheldrick, *Acta Crystallogr., Sect. A: Found. Crystallogr.*, 2015, **71**, 3; (*b*) G. M. Sheldrick, *Acta Crystallogr., Sect. C: Struct. Chem.*, 2015, **71**, 3.